Composite Structures 303 (2023) 116332

Contents lists available at ScienceDirect

Composite Structures

journal homepage: www.elsevier.com/locate/compstruct

Multi-level micromechanics-based homogenization for the prediction of damage behavior of multiscale fiber-reinforced composites

Taegeon Kil [a], Jin-Ho Bae [a], Beomjoo Yang [b], H.K. Lee [a,*]

[a] Department of Civil and Environmental Engineering, Korea Advanced Institute of Science and Technology (KAIST), 291 Daehak-ro, Yuseong-gu, Daejeon 34141, South Korea
[b] School of Civil Engineering, Chungbuk National University, 1 Chungdae-ro, Seowon-gu, Cheongju, Chungbuk 28644, South Korea

ARTICLE INFO

Keywords:
Fiber-reinforced composites
Micromechanics
Molecular dynamics
Homogenization
Carbon nanotube

ABSTRACT

A multi-level micromechanics-based homogenization is proposed here to investigate the damage behavior of composites with multiscale fibers such as carbon nanotube (CNT) and carbon fiber. First, a molecular unit cell is constructed considering the interfacial characteristics between the CNT and a polymer matrix, after which molecular dynamics simulation and micromechanics are utilized to obtain the elastic properties of CNT-reinforced composites. A micromechanics-based progressive damage model is then adopted to predict the damage behavior of the CNT and carbon fiber-reinforced composites. Tensile tests are also conducted to investigate the stress–strain behaviors of the composites. To verify the applicability of the proposed model, the present predictions are compared with those obtained from the tensile test results. The proposed multi-level homogenization has shown to provide a close match to the experimental results. The proposed modeling scheme may facilitate a thorough investigation of the damage behavior of multiscale fiber-reinforced composites, proving the importance of each constituent at a different level.

1. Introduction

Carbon fiber-reinforced composites have been utilized for principal structural components in the aircraft, automobile, and infrastructure industries. These materials have useful engineering properties (e.g., superior stiffness and specific strength, corrosion resistance, fatigue resistance, and low density), allowing reductions of product weights by replacing increasingly more metal parts [1,2]. Recently, many studies have focused on the incorporation of nanoscale fiber materials into carbon fiber-reinforced composites for the development of highly functional and advanced composite materials [3–6]. These types of multiscale fiber-reinforced composites can improve mechanical performance outcomes and serve as cost-effective composite materials by optimizing the content of fibers of different scales [7].

Carbon nanotube (CNT) is considered to be a potential candidate for the manufacturing of multiscale fiber-reinforced composites owing to their low density, high aspect ratio, and excellent mechanical properties [8–11]. The tensile strength and elastic modulus of a typical CNT are as high as 150 GPa and 1.0 TPa, respectively, due to the sp^2 chemical structure of the carbon atoms in the CNT, which provide strong bonding force exceeding that of steel [12–14]. Lee et al. [15] introduced CNT between carbon fiber-reinforced composites, reporting that their composites showed improved tensile strength and elastic modulus outcomes by 20.0% and 31.0%, respectively, compared to those of conventional carbon fiber-reinforced composites. Abidin et al. [16] developed carbon fiber-reinforced composites with CNT. They reported that the fracture toughness of the developed composites increased by 41.0% compared to that of composites without CNT [16].

Meanwhile, the greatest challenge posed by multiscale fiber-reinforced composites is that they show great differences in mechanical performance outcomes due to the inherent characteristics of fibers of the vastly different scales [17]. Accordingly, accurate analyses and simulations of the complete responses of components and systems in multiscale fiber-reinforced composites are essential. Over the years, several other researchers have proposed theoretical modeling approaches using micromechanics and molecular dynamics (MD) simulations to evaluate and design composites with fibers of various scales more accurately [18–23].

Alian et al. [19,23] developed a multiscale modeling technique that combines the Mori-Tanaka method and MD simulation for determining the effective elastic modulus of CNT-reinforced composites. They reported that their model can consider the effect of interfacial properties

* Corresponding author.
E-mail address: haengki@kaist.ac.kr (H.K. Lee).

https://doi.org/10.1016/j.compstruct.2022.116332
Received 7 April 2022; Received in revised form 8 August 2022; Accepted 7 October 2022
Available online 13 October 2022
0263-8223/© 2022 Published by Elsevier Ltd.

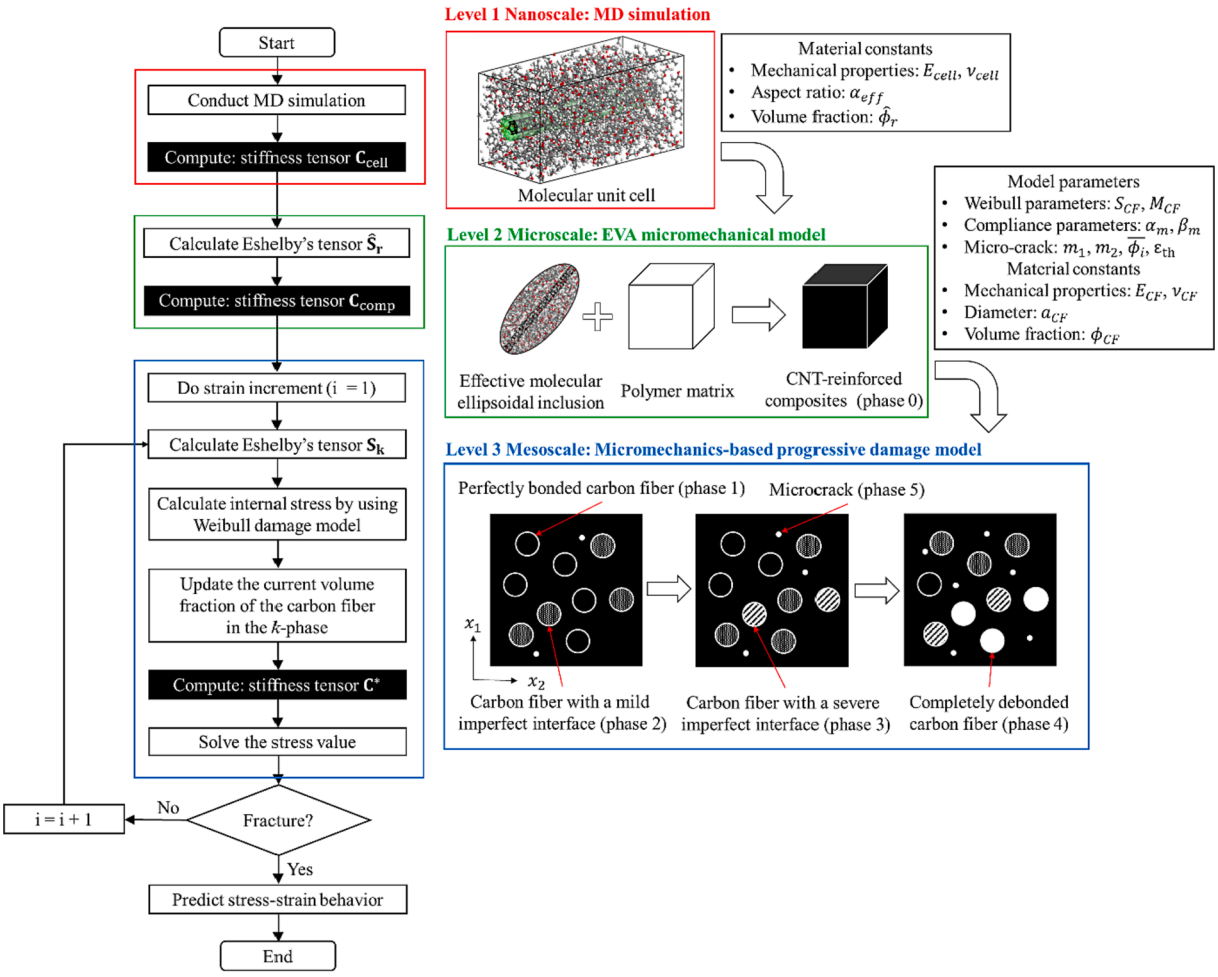

Fig. 1. Flowchart of the proposed multi-level micromechanics-based homogenization scheme for CNT and carbon fiber-reinforced composites (cf. [19,24]).

and agglomeration of CNT on the elastic properties of the composites [19,23]. Radue et al. [20] proposed a multiscale modeling approach to characterizing the mechanical properties of multiscale fiber-reinforced composites by means of an MD simulation integrated with micromechanics. Their modeling approach can generate fairly reasonable estimations of the elastic modulus of composites considering the presence of interphase and interfacial imperfections [20]. Despite several studies that focus on the prediction of the effective mechanical properties of multiscale fiber-reinforced composites, a comprehensive investigation of multiscale fiber-reinforced composites to investigate the damage behavior of these composites has yet to be conducted.

Hence, this prompted us to propose a multi-level micromechanics-based homogenization to predict the damage behavior of multiscale fiber-reinforced composites. The present study suggests a multi-level homogenization scheme that includes MD simulations and a series of micromechanical models. First, a molecular unit cell is constructed considering the interfacial characteristics between the CNT and polymer matrix, after which the MD simulation and micromechanics are utilized to obtain the elastic properties of CNT-reinforced composites. Next, this study adopts a micromechanics-based progressive damage model to predict the damage behavior of the CNT and carbon fiber-reinforced composites. Tensile tests are conducted to investigate the stress–strain behaviors of the composites. To verify the predictive capability of the proposed model, the predicted stress–strain behaviors of the composites are compared with experimentally derived results.

2. Theoretical modeling

Let us consider composites consisting of CNT, carbon fiber, and a polymer matrix. Fig. 1 shows a flowchart of the proposed multi-level micromechanics-based homogenization scheme for CNT and carbon fiber-reinforced composites (cf. [19,24]). This study proposes a three-level homogenization to predict the damage behavior of CNT and carbon fiber-reinforced composites. At Level 1, a molecular unit cell based on MD is constructed to estimate the mechanical properties of the effective molecular ellipsoidal inclusion, after which micromechanics is utilized to obtain the elastic properties of CNT-reinforced composites at Level 2. At Level 3, a micromechanics-based progressive damage model [24,25] is adopted to predict the stress–strain behavior of the CNT and carbon fiber-reinforced composites.

At Level 1, an MD simulation is conducted to estimate the mechanical properties of an effective molecular ellipsoidal inclusion. At this level, the MD simulation is performed using the commercial molecular dynamics simulation package Materials Studio, with the COMPASS forcefield. Fig. 2 shows the molecular unit cell of the CNT-reinforced composites utilized in the present MD simulation (cf. [18,19]). A centered CNT is modeled as a segregate with an isosurface to consider Coulombic forces and van der Waals interactions between the CNT and epoxy atoms. It was reported that Alian et al. [19,23], who constructed the representative volume element of CNT-reinforced composites by means of MD simulation, assumed a CNT content within the range of 6.5–12.2 vol.% to determine the effective elastic properties of these types of composites. According to the previous studies [18,19,23], a molecular unit cell with a 10 vol.% of CNT is constructed here with

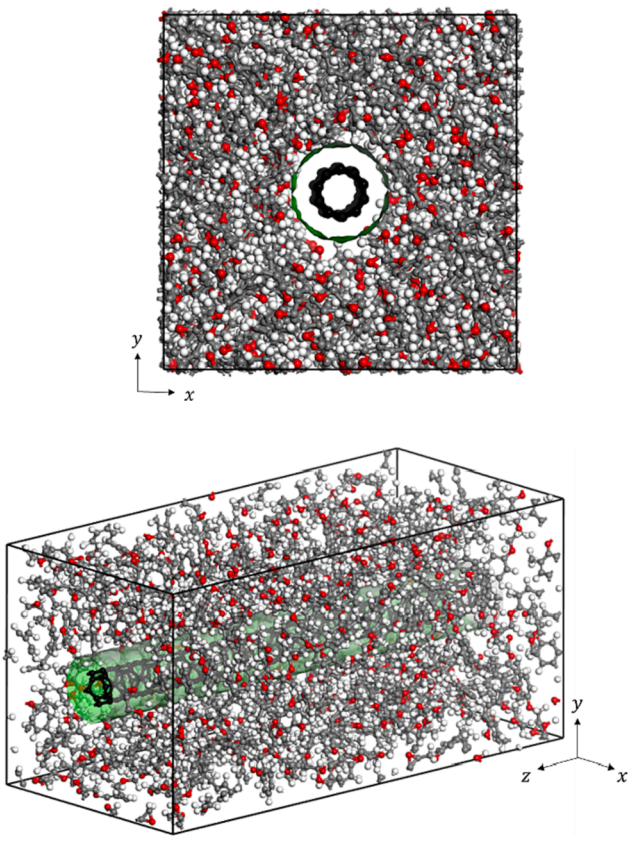

Fig. 2. The molecular unit cell of the CNT-reinforced composites utilized in the present MD simulation (cf. [18,19]).

Table 1
Model parameters and conditions in the present MD simulation.

Parameter and condition	Present simulation
Forcefield	COMPASS
CNT volume fraction (vol.%)[a]	10.0
Cell size (Å^3)[a]	30 × 30 × 63.9
Target density (g/cm^3)	1.0
MD ensemble simulation	NVT and NPT
Temperature (K)	298.0
Temperature control	Nosé–Hoover-Langevin
Pressure (GPa)	0.0001
Pressure control	Berendsen
Total number of atoms	4600

[a] Note that the values of the parameters are determined by referring to the previous studies (cf. [18,19,23]).

periodic boundary conditions imposed in all directions. The volume fraction of CNT is calculated by dividing the volume of the segregate of the CNT by the total molecular unit cell volume (30 Å × 30 Å × 63.9 Å) [19]. In this case, 100 epoxy oligomers are packed into the isosurface-enclosed volume with a target density of 1.0 g/cm^3. The model parameters and conditions in the present MD simulation are listed in Table 1.

The total potential energy of the initial configuration is minimized via a conjugate gradient algorithm with a specific maximum energy change of 0.001 kcal/mol [18]. After sufficiently minimizing the initial molecular unit cell, the molecular unit cell is equilibrated at 298.0 K via a canonical, *NVT*, ensemble simulation [18]. The molecular unit cell is then equilibrated again at 298.0 K and 0.0001 GPa via an isobaric-isothermal canonical, *NPT,* ensemble simulation. After the equilibrium process is complete, uniaxial compression is conducted to determine the mechanical properties of the molecular unit cell. Strain-controlled compression of 0.1% is applied along the *z*-direction by consistently compressing the molecular unit cell updating the atoms' coordinates under the compressed lattice box. The molecular unit cell is equilibrated between strain intervals using the *NPT* ensemble simulation at 298 K and 0.0001 GPa. The time-averaged virial stress derived from the virial theorem is stored as the stress components corresponding to the strain state. This procedure is repeated until the strain of the molecular unit cell reaches an elastic limit of 3.0% [19].

It should be noted that the present MD simulation assumes straight CNT without waviness or aggregation of the CNT in the polymer matrix. Accordingly, the present modeling scheme cannot consider the aggregation of CNT. Furthermore, a single-walled CNT with anisotropic epoxy oligomers is modeled in this study with periodic boundary conditions due to computational constraints when considering the significant number of atoms in the MD simulation. Therefore, repetitive calculations are conducted and averaging schemes are utilized to improve the computational accuracy of the MD simulation [18].

After MD simulation on the molecular unit cell at Level 1, to obtain the elastic properties of the CNT-reinforced composites, the ensemble volume averaging (EVA) micromechanical model proposed by Ju and Chen [26] is adopted at Level 2. Two-phase composites consisting of a polymer matrix (matrix phase) and an effective molecular ellipsoidal inclusion (inclusion phase) are considered. Note that the elastic modulus E_{cell} and Poisson's ratio ν_{cell} of the molecular unit cell are inputted as the properties of the materials of the effective molecular ellipsoidal inclusion as shown in Fig. 1. According to the EVA model for non-interacting; randomly dispersed; and similar spheroidal inclusions, the stiffness tensor is given as follows [26,27]:

$$\mathbf{C}_{\mathbf{comp}} = \widehat{\mathbf{C}}_0 \bullet \left[\mathbf{I} + \sum_{r=1}^{2} \left[\widehat{\phi}_r (\widehat{\mathbf{A}}_\mathbf{r} + \widehat{\mathbf{S}}_\mathbf{r})^{-1} \bullet \left\{ \mathbf{I} - \widehat{\phi}_r \widehat{\mathbf{S}}_\mathbf{r} \bullet (\widehat{\mathbf{A}}_\mathbf{r} + \widehat{\mathbf{S}}_\mathbf{r})^{-1} \right\}^{-1} \right] \right] \tag{1}$$

with.

$$\widehat{\mathbf{A}}_\mathbf{r} = (\widehat{\mathbf{C}}_\mathbf{r} - \widehat{\mathbf{C}}_0)^{-1} \bullet \widehat{\mathbf{C}}_0 \tag{2}$$

where $\mathbf{I}$ and $\widehat{\mathbf{C}}_0$ are the identity tensor and fourth-rank stiffness tensor for the matrix, respectively; $\widehat{\phi}_r$, $\widehat{\mathbf{S}}_\mathbf{r}$, and $\widehat{\mathbf{A}}_\mathbf{r}$ are the volume fraction, fourth-rank Eshelby's tensor, and fourth-rank elasticity tensor of a *r*-phase inclusion, respectively [26–28]. In this study, all effective molecular ellipsoidal inclusions are initially modeled assuming they are randomly oriented with a prolate spheroidal shape and a perfect interface condition. The general forms of the Eshelby's tensor can be found in Pyo and Lee (2009) [29]. Note that the aspect ratio of the effective molecular ellipsoidal inclusion α_{eff} is defined as $\alpha_{eff} = l_{eff}/d_{eff}$, using the material properties of CNT in an experimental program, where l_{eff} and d_{eff} are the radius of the prolate spheroid on the major and minor axis, respectively.

At Level 3, a micromechanics-based progressive damage model is adopted to predict the stress–strain behavior of the CNT and carbon fiber-reinforced composites [24,25]. The unidirectional carbon fiber in the polymer matrix is aligned and randomly distributed. Here, we consider CNT and carbon fiber-reinforced composites consisting of CNT-reinforced composites (phase 0), transversely elastic continuous types of carbon fiber (phases 1, 2, 3, and 4), and a microcrack (phase 5), as shown in Fig. 1 [24,25]. In accordance with Lee and Pyo (2009) [24], as deformations continue to increase, some initially perfectly bonded carbon fibers (phase 1) are transformed to carbon fibers with a mild imperfect interface (phase 2); some carbon fibers with a mild imperfect interface are then transformed to carbon fibers with a severe imperfect interface (phase 3); and all carbon fibers are transformed to completely debonded carbon fibers (phase 4) which are regarded as cylindrical voids. Moreover, microcracks (phase 5) are nucleated asymptotically as randomly dispersed spherical voids [24].

With the help of the fourth-rank Eshelby tensor, the elasticity tensor

for 5-phase composites containing unidirectionally aligned carbon fiber $\mathbf{C}^*$ can be expressed as Eq. (3) with Eq. (4), as reported in the earlier works [24,30,31]:

$$\mathbf{C}^* = \mathbf{C_{comp}} \bullet \left[\mathbf{I} + \sum_{k=1}^{5} \left[\phi_k (\mathbf{A_k} + \mathbf{S_k})^{-1} \bullet \left\{ \mathbf{I} - \phi_k \mathbf{S_k} \bullet (\mathbf{A_k} + \mathbf{S_k})^{-1} \right\}^{-1} \right] \right] \tag{3}$$

with.

$$\mathbf{A_k} \equiv \left(\mathbf{C_k} - \mathbf{C_{comp}} \right)^{-1} \bullet \mathbf{C_{comp}} \tag{4}$$

where $\mathbf{C_k}$ and ϕ_k denote the fourth-rank elasticity tensor and volume fraction of a k-phase inclusion, respectively, and $\mathbf{S_k}$ is the fourth-rank Eshelby's tensor for the k-phase [24]. Note that $\mathbf{C_{comp}}$ is estimated by inputting the results calculated by Eq. (1).

The interfacial layer properties between the matrix and carbon fiber are modeled by adopting the interface modeling scheme proposed by Qu [32]. According to this modeling scheme, the interface is modeled as a linear spring layer of disappearing thickness, which is represented by a second-rank compliance tensor η_{ij} [32]. The modified Eshelby's tensor $\mathbf{S_{m+1}}$ using η_{ij} for the composites can be estimated by Eqs. (5) and (6) [24,32,33]:

$$\eta_{ij} = \alpha_m \delta_{ij} + (\beta_m - \alpha_m) n_i n_j \tag{5}$$

and.

$$(S_{m+1})_{ijkl} = \frac{1}{256 a_{CF} (1 - \nu_{comp})} \left[S_{IK}^{M(2m-1)} \delta_{ij} \delta_{kl} + S_{IJ}^{M(2m)} \left(\delta_{ik} \delta_{jl} + \delta_{il} \delta_{jk} \right) \right] \tag{6}$$

where α_m and β_m ($m = 1$ and 2) are used as model parameters with 1 indicating a mild imperfect interface and 2 indicating a severe imperfect interface; a_{CF} and ν_{comp} denotes the radius of the cross-section of the carbon fiber and Poisson's ratio of the CNT-reinforced composites; and δ_{ij}, n_i, and n_j denote the Kronecker delta, unit outward normal vector and unit tangential vector, respectively [24,32,33]. The components of second-rank tensors $S_{IK}^{M(2m-1)}$ and $S_{IJ}^{M(2m)}$ are given in Lee and Pyo (2009) [24].

A damage model proposed earlier [34,35] is adopted in the present study. The progressive damage model of the composites can be expressed by Eq. (7) with Eq. (8) as the current volume fraction of carbon fiber in the k-phase using the Weibull probability function [34,35]:

$$\begin{aligned} \overline{\phi}_2 &= \phi_{CF} \left\{ 1 - \exp\left(- \frac{\left((\overline{\sigma}_{11})_{\mathrm{CF}} \right)_m}{S_{CF}} \right)^{M_{\mathrm{CF}}} \right\}, \\ \overline{\phi}_3 &= \overline{\phi}_2 \left\{ 1 - \exp\left(- \frac{\left((\overline{\sigma}_{11})_{\mathrm{CF}} \right)_m}{S_{CF}} \right)^{M_{\mathrm{CF}}} \right\}, \\ \phi_4 &= \overline{\phi}_3 \left\{ 1 - \exp\left(- \frac{\left((\overline{\sigma}_{11})_{\mathrm{CF}} \right)_m}{S_{CF}} \right)^{M_{\mathrm{CF}}} \right\} \end{aligned} \tag{7}$$

with.

$$\phi_3 = \overline{\phi}_3 - \phi_4, \ \phi_2 = \overline{\phi}_2 - \overline{\phi}_3, \ \phi_1 = \phi_{CF} - \overline{\phi}_2 \tag{8}$$

Here, ϕ_{CF} and $\left((\overline{\sigma}_{11})_{\mathrm{CF}} \right)_m$ are the original volume fraction of the carbon fiber and the average internal stress in the transverse direction of the carbon fiber (phase 1), respectively; S_{CF} and M_{CF} are the Weibull parameters in the progressive damage model [34]. For uniaxial loading in the longitudinal direction, $\left((\overline{\sigma}_{11})_{\mathrm{CF}} \right)_m$ can be replaced with $\left((\overline{\sigma}_{33})_{\mathrm{CF}} \right)_m$. The internal stresses of the carbon fiber required for the initiation of an imperfect interface are explicitly expressed as Eq. (9), as follows [36]:

Table 2
Parameters utilized in the micromechanics-based simulation for CNT-reinforced composites.

Parameter	Present simulation
Elastic modulus of matrix E_0 (GPa)	1.87
Poisson's ratio of matrix ν_0	0.38
Elastic modulus of effective inclusion E_{cell} (GPa)	64.75
Poisson's ratio of effective inclusion ν_{cell}	0.34
Diameter of effective inclusion[a] d_{eff} (nm)	26.0
Length of effective inclusion[a] l_{eff} (μm)	10.0
Aspect ratio of effective inclusion[a] α_{eff}	384.6
Volume fraction of matrix $\widehat{\phi_1}$ (vol.%)	95.0
Volume fraction of effective inclusion $\widehat{\phi_2}$ (vol.%)	5.0

[a] Note that the values of the parameters are determined by referring to the previous studies (cf. [7]).

$$\begin{aligned} (\overline{\sigma}_{11})_{\mathbf{CF}} &= \mathbf{C}_1 \bullet \left[\mathbf{I} - \mathbf{S}_1 \bullet (\mathbf{A}_1 + \mathbf{S}_1)^{-1} \right] \bullet \left[\mathbf{I} - \sum_{k=1}^{4} \left\{ \phi_k \mathbf{S}_k \bullet (\mathbf{A}_k + \mathbf{S}_k)^{-1} \right\} \right]^{-1} \\ &\quad : \overline{\boldsymbol{\varepsilon}} \\ &= \left[U_{IK}^{(1)} \delta_{ij} \delta_{kl} + U_{IJ}^{(2)} \left(\delta_{ik} \delta_{jl} + \delta_{il} \delta_{jk} \right) \right] : \overline{\boldsymbol{\varepsilon}} \end{aligned} \tag{9}$$

where the components of the tensors $U_{IK}^{(1)}$ and $U_{IJ}^{(2)}$ can be found in Ju and Lee (2001) [36].

In addition, a crack nucleation model [37,38] is adopted here for simulating microcracks nucleation in brittle materials. The volume fraction of microcracks ϕ_5 can be defined by Eq. (10) [37,38]:

$$\phi_5 = \begin{cases} \overline{\phi}_i, & (\varepsilon^{\mathrm{eff}} \le \varepsilon_{\mathrm{th}}) \\ \overline{\phi}_i + m_1 \left(1 - \dfrac{\varepsilon_{\mathrm{th}}}{\varepsilon^{\mathrm{a}}} \right)^{m_2}, & (\varepsilon^{\mathrm{eff}} > \varepsilon_{\mathrm{th}}) \end{cases} \tag{10}$$

where $\overline{\phi}_i$, $\varepsilon^{\mathrm{eff}}$, and $\varepsilon_{\mathrm{th}}$ are the initial density of microcracks, current accumulated effective macroscopic strain, and effective strain threshold below which no nucleation take place, respectively. m_1 and m_2 the material parameters depending on the specific shape and distribution of microcracks, respectively [37,38].

3. Simulation results and parametric investigation

3.1. Effects of the effective molecular ellipsoidal inclusion orientation and geometry

The simulation results and parametric investigation at each level of the materials are discussed subsequently. The MD simulation of the molecular unit cell at Level 1 provides $E_{cell} = 64.75$ GPa and Poisson's ratio $\nu_{cell} = 0.34$. These values obtained by the MD simulation can be acceptable when compared to values from the literature when an MD simulation was utilized [19,20,39]. These values are considered as input parameters to determine the elastic properties of the effective molecular ellipsoidal inclusion in the present theoretical modeling.

Based on the parameters presented in Table 2, the effects of the effective molecular ellipsoidal inclusion orientation and geometry at Level 2 are investigated. Fig. 3(a) shows the predicted elastic moduli of CNT-reinforced composites E_{comp} with various CNT contents of the effective molecular ellipsoidal inclusion. Note that the Aligned_33 and Aligned_11 cases indicate E_{comp} in the longitudinal and transverse directions, respectively. The elastic moduli of the Aligned_33 case as a transversely isotropic material are higher than those of the Random and Aligned_11 cases. It can be said from these results that the inclusion orientation has a significant effect on the elastic modulus of these composites as reported elsewhere [29,33].

Fig. 3(b) shows the predicted elastic moduli of CNT-reinforced composites E_{comp} with various aspect ratios of the effective molecular

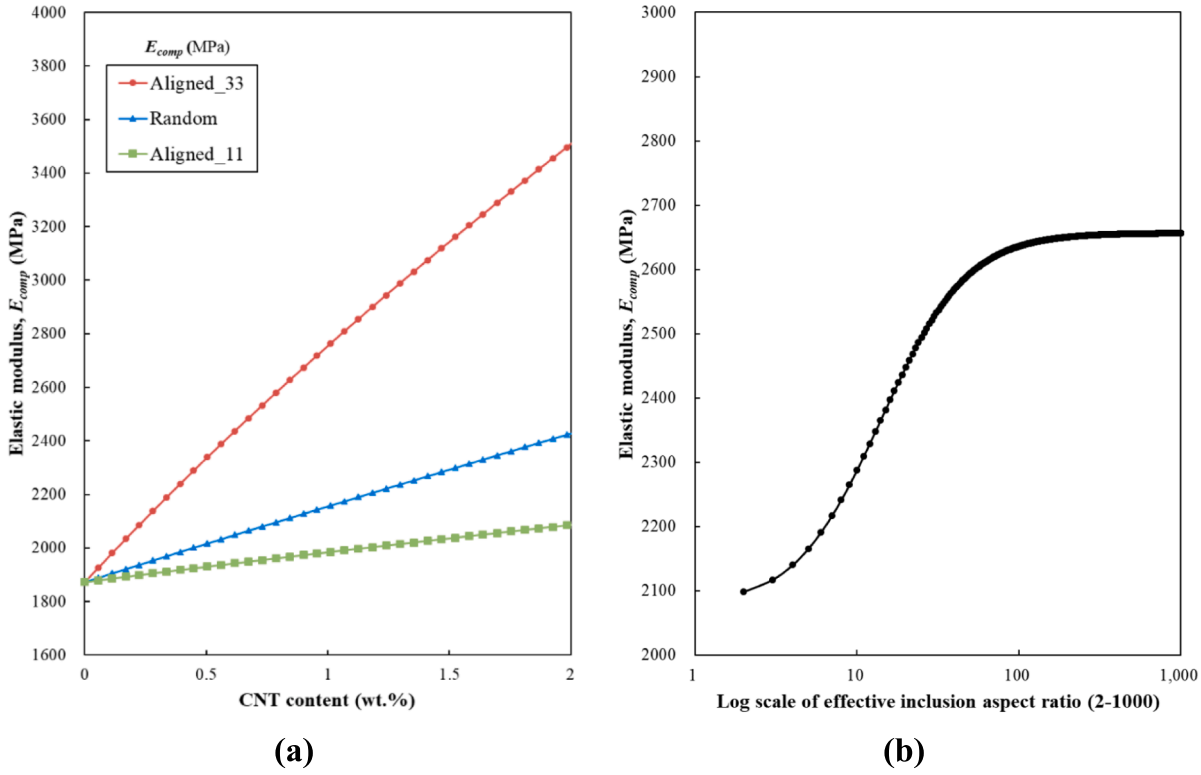

Fig. 3. Predicted elastic moduli of CNT-reinforced composites with (a) various CNT contents and (b) various aspect ratios of the effective molecular ellipsoidal inclusion.

Table 3
Parameters utilized in the micromechanics-based simulation for CNT and carbon fiber-reinforced composites.

Parameter	Present simulation
Elastic modulus of CNT-reinforced composites E_{comp} (GPa)	2.0
Poisson's ratio of CNT-reinforced composites ν_{comp}	0.3
Elastic modulus of CF E_{CF} (GPa)	210
Poisson's ratio of CF ν_{CF}	0.2
Radius of CF a_{CF} (μm)	0.5
Volume fraction of CF ϕ_{CF} (vol.%)	25
Weibull parameter[a] S_{CF} and M_{CF}	400 and 1.0
Compliance parameter[a] α_1, β_1, α_2, and β_2	2.0, 3.0, 2.0E-7, and 3.0E-7
Microcrack parameter[a] m_1, m_2, $\overline{\phi_i}$, and ε_{th}	0.25, 1.6, 0.05, and 0.002

[a] Note that the values of the parameters are determined by referring to the previous studies (cf. [24,25]).

ellipsoidal inclusion. Two different trends in the change of E_{comp} with varying the aspect ratio become evident. In the first range, referring to inclusions with an aspect ratio varying from 2 to 100, E_{comp} increases noticeably as the aspect ratio approaches 100. Then, E_{comp} becomes constant in the second range from 100 to 1000. This result indicates that a higher aspect ratio of effective molecular ellipsoidal inclusion is expected to provide much higher stiffness to the composites.

3.2. Effects of the elastic modulus of CNT-reinforced composites and carbon fiber volume fraction

A series of parametric studies are conducted to evaluate the degree of sensitivity of the proposed multi-level homogenization scheme to the effect of the elastic modulus of CNT-reinforced composites E_{comp} and the volume fraction of carbon fiber ϕ_{CF}. The present parametric studies demonstrate stress–strain behaviors under uniaxial tension. In these numerical studies, the parameters utilized in micromechanics-based simulations for CNT and carbon fiber-reinforced composites are presented in Table 3.

The predicted stress–strain behaviors of CNT and carbon fiber-reinforced composites under uniaxial tension with varying the values of E_{comp} and ϕ_{CF} are shown in Fig. 4. As E_{comp} increases, the stress in the longitudinal direction increases from 0.001 strain, while the stress in the transverse direction is increased from the initial stage, as shown in Fig. 4 (a) and (b), respectively. Fig. 4(c) and (d) demonstrate that the stress in the composites improves as ϕ_{CF} increases in all directions. Particularly, the stress in the longitudinal direction increases significantly as the strain increases, with the stress–strain behavior of the composites becoming stiffer. The results in Fig. 4 indicate that a higher E_{comp} has a significant effect on the stress–strain behavior in the transverse direction, while a higher ϕ_{CF} has an important effect on this behavior in the longitudinal direction.

3.3. Effects of the Weibull parameter and carbon fiber interfacial properties

An additional parametric study is performed to predict the stress–-strain behaviors of the CNT and carbon fiber-reinforced composites, reflecting the effects of the Weibull parameter S_{CF} and compliance parameters with the severely imperfect interfaces α_2 and β_2. The other parameters are identical to those used in Section 3.2. The predicted stress–strain behaviors of CNT and carbon fiber-reinforced composites under uniaxial tension with varying the values of S_{CF}, α_2, and β_2 are shown in Fig. 5(a) and (b). The range of S_{CF} is from 400 to 800, while α_2 and β_2 remain constant at 2.0E-7 and 3.0E-7, respectively. In Fig. 5(b), the ranges of α_2 and β_2 are from 2.0−2.0E-9 and 3.0–3.0E-9, respectively, while S_{CF} remains constant at 400 [24]. Fig. 5(c) exhibits the predicted damage evolution of the carbon fiber volume fraction corresponding to Fig. 5(a).

As shown in Fig. 5(a), a higher value of S_{CF} leads to slower evolution

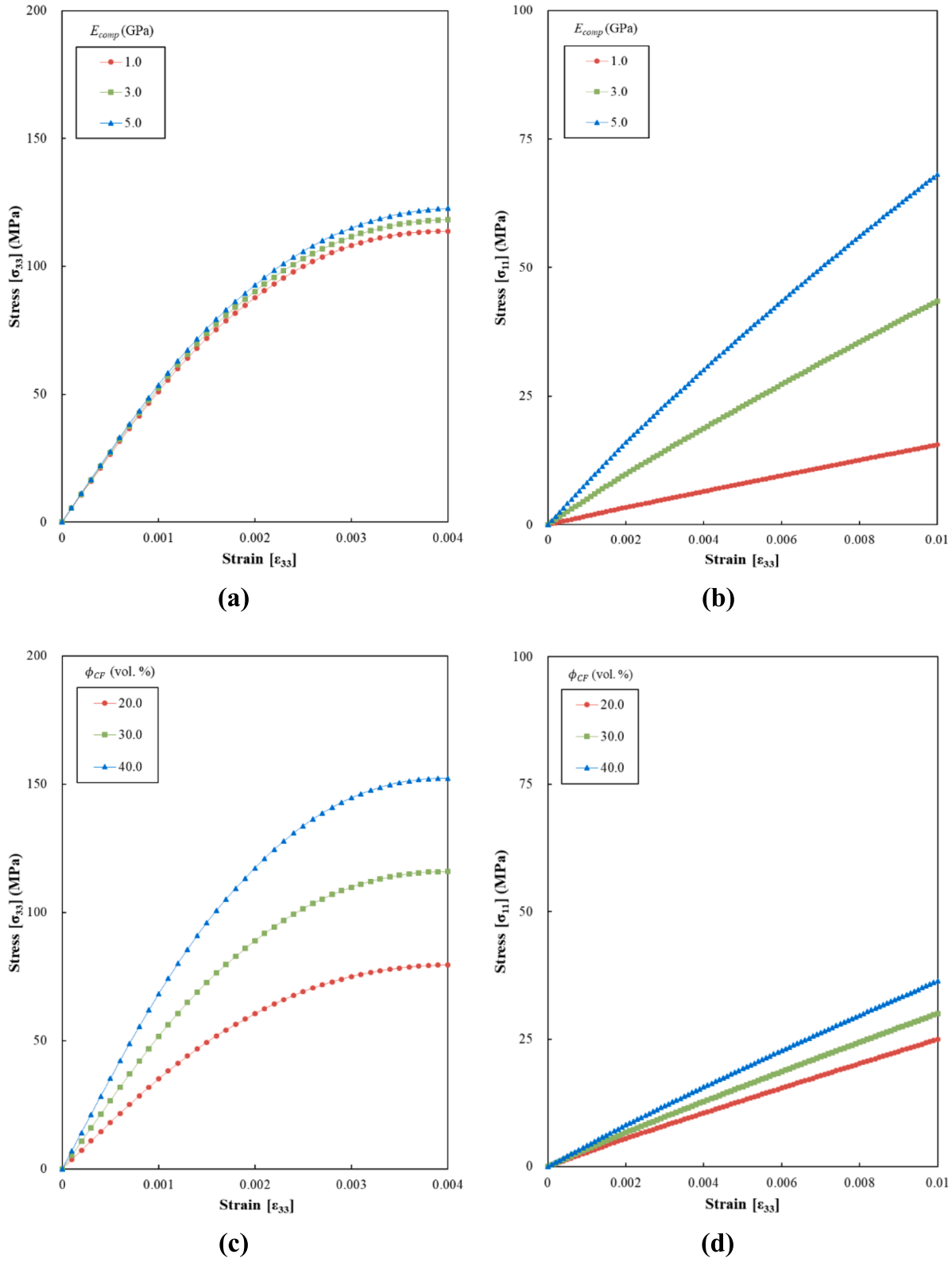

Fig. 4. Predicted stress–strain behaviors of CNT and carbon fiber-reinforced composites under uniaxial tension: (a) longitudinal and (b) transverse directions with varying E_{comp}, and (c) longitudinal and (d) transverse directions with varying..ϕ_{CF}

of an imperfect interface in the longitudinal direction. These results indicate that the carbon fiber in their interfaces resists at a later stage as S_{CF} increases. From Fig. 5(c), it is clear that a higher value of S_{CF} leads to slower evolution of an imperfect interface, indicating that S_{CF} plays an important role in determining the progressive damage stage in carbon fiber interfaces. In addition, the values of α_2 and β_2 would approach ∞ ($\alpha_2 = \beta_2 \rightarrow \infty$) at a completely debonded interface of carbon fiber, whereas, at a perfectly bonded interface of carbon fiber, the values of α_2 and β_2 would approach 0 ($\alpha_2 = \beta_2 \rightarrow 0$) [33]. Therefore, the overall stress value of the composites gradually increases as the values of α_2 and β_2

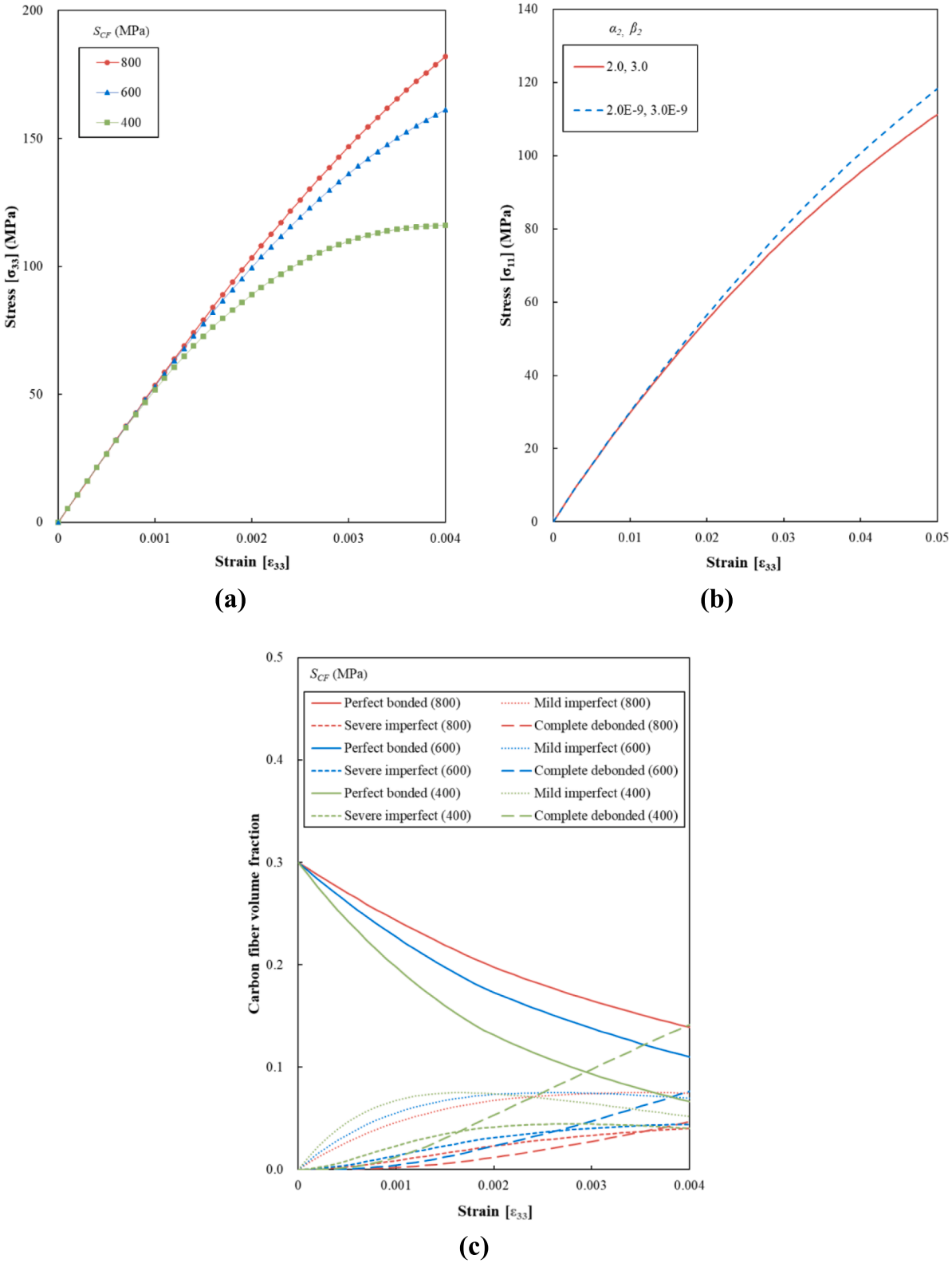

Fig. 5. Predicted stress–strain behaviors of CNT and carbon fiber-reinforced composites under uniaxial tension: (a) longitudinal direction with varying S_{CF}, (b) transverse direction with varying α_2 and β_2; and (c) the predicted damage evolution of the carbon fiber volume fraction corresponding to (a).

decrease, as depicted in Fig. 5(b). The effect of the imperfect carbon fiber interface on the stress–strain behaviors of the composites is noticeable under 0.05 strain in the transverse direction. These results indicate that S_{CF}, α_2, and β_2 have a significant effect on the overall damage behavior of these types of composites.

4. Model verification

4.1. Experimental program

To verify the applicability of the proposed model, tensile tests of the

Table 4
Mix proportions of the CNT and carbon fiber-reinforced composites (wt.%).

Composites*	Epoxy Base	Curing agent	CNT	PSS	Carbon fiber-reinforced prepreg
0-CNT	100	25	0	1.0	0
0.1-CNT	100	25	0.1	1.0	0
0.2-CNT	100	25	0.2	1.0	0
0.3-CNT	100	25	0.3	1.0	0
0.4-CNT	100	25	0.4	1.0	0
0-CNT/CF-33	100	25	0	1.0	25
0-CNT/CF-11	100	25	0	1.0	25
0.2-CNT/CF-33	100	25	0.2	1.0	25
0.2-CNT/CF-11	100	25	0.2	1.0	25

* Note that the digits included in the composites' names successively denote their CNT content (wt.%) and the direction of the carbon fiber in the carbon fiber-reinforced prepreg.

CNT and carbon fiber-reinforced composites are conducted. CNT (K-Nanos 100P, Kumho Petrochemical, Co.) having a bulk density of 0.02 g/cm^3 and purity of $>$ 90% is used in this study. The length and diameter of the CNT are approximately 10.0 μm and 26.0 nm, respectively. An epoxy base having a density of 1.2 g/cm^3 and a corresponding curing agent (Poonlim Industrial Co., Ltd.) are used to compose the polymer matrix. The elastic modulus and Poisson's ratio of the hardened epoxy are 1.87 GPa and 0.38, respectively. Poly(sodium 4-styrenesulfonate) (PSS) is chosen as a dispersant to improve the dispersion of the CNT particles in the polymer matrix [40]. A carbon fiber-reinforced epoxy prepreg (Hankuk Carbon Co., Ltd.) with a density of 1.4 g/cm^3 and thickness of 0.63 mm is used. The elastic modulus, Poisson's ratio, and diameter of the carbon fiber in the prepreg are 210 GPa, 0.2, and 1.0 μm, respectively. The size of the composites corresponds to ASTM D638-14 (Type I) [41] with a thickness of 10 mm. Here, nine different mix proportions are used to fabricate the composites considering the content of the CNT, as summarized in Table 4. The CNT and PSS contents are referenced from the previous studies [40,42]. Note that the digits included in the composites' names denote their CNT contents (wt.%) and the direction of the carbon fiber in the prepreg, respectively; i.e., 0.2-CNT/CF-33 represents composites with a content of 0.2 wt.% CNT with carbon fiber in the longitudinal direction.

Schematics of the fabrication procedure of the CNT and carbon fiber-reinforced composites used in the tensile test are shown in Fig. 6. The CNT and carbon fiber-reinforced composites are fabricated as follows. First, CNT, PSS, and an epoxy base are added to isopropyl alcohol (IPA) as a solvent, after which the mixture is physically agitated by hand for 1 min. The mixture is then sonicated with a tip-type ultrasonicator for one hour (200 W and 40 kHz) [43], and the CNT-dispersed solution is heated to 130 ℃ and mixed by means of mechanical stirring at 200 rpm using a magnetic stirrer to evaporate the IPA solvent completely. After evaporating the IPA solvent, an epoxy curing agent is added to the mixture, and this is hand-mixed for 1 min. For the CNT series composites without carbon fiber, the CNT-dispersed epoxy mixture is shallowly poured into the mold for the tensile test. For the CNT and carbon fiber-reinforced composites, ten prepregs are laminated in the mold by pasting in a CNT-dispersed epoxy mixture, minimizing air voids between the interlayers. Here, for the composites reinforced by carbon fiber in the transverse direction, the carbon fiber-reinforced prepreg is laminated on the mold in the transverse direction. The composites are heated in an autoclave for one hour at a temperature of 130 ℃ [44], after which they are cooled to room temperature and cured at that temperature for one week.

The effect of the addition of CNT and carbon fiber on the stress–strain behavior is evaluated by means of tensile tests in accordance with ASTM D3039/D3039M [45] using a universal testing machine (UTM). A UTM with a maximum loading capacity of ten tons is used with a maximum crosshead speed of 0.75 mm/min. The strain is measured using a bi-axial strain gauge with a gauge resistance value of 118.5 ± 0.5 Ω and gauge factor of 2.08 ± 1% (Tokyo Measuring Instruments Laboratory Co., Ltd.). The strain rate is held constant at 0.001 s^{-1} according to the quasi-static tensile loading state.

4.2. Comparisons between experimental results and the present predictions

Fig. 7 presents the measured stress–strain behaviors of the CNT-reinforced composites. The increases in the ultimate tensile strength of the 0.1, 0.2, and 0.3-CNT composites exceed that of the 0-CNT composites. The ultimate tensile strength outcomes of the 0.1-CNT and 0.2-CNT composites are respectively 22.1 and 23.0 MPa, corresponding to increases of 9.4% and 13.8%. The stress–strain behavior of the 0.4-CNT composites shows the steepest slope and the highest stress value under the 0.008 strain condition. This result indicates that the addition of CNT in the range of 0.1–0.3 wt.% effectively enhances the slope and ultimate tensile strength compared to the outcomes with 0-CNT composites. It is well known that the addition of small content of well-dispersed CNT improves the mechanical properties of the composites [8,46]. Thus, it can be inferred from the results that the present fabrication method as shown in Fig. 6 seems to be appropriate to manufacture the CNT-reinforced composites, leading to the improved mechanical properties of these composites.

Comparisons of the elastic moduli and Poisson's ratios of the CNT-reinforced composites E_{comp} and ν_{comp} between the experimental results and the present predictions are shown in Fig. 8. In the present study, three different types of composites are manufactured with different CNT contents, and the mean values from the experimental results are compared with the present predictions. The methods adopted and model parameters for the prediction are identical to those used in Section 3.1. As the content of CNT increases, both the experimental and predicted values of E_{comp} are increased except for the 0.3-CNT

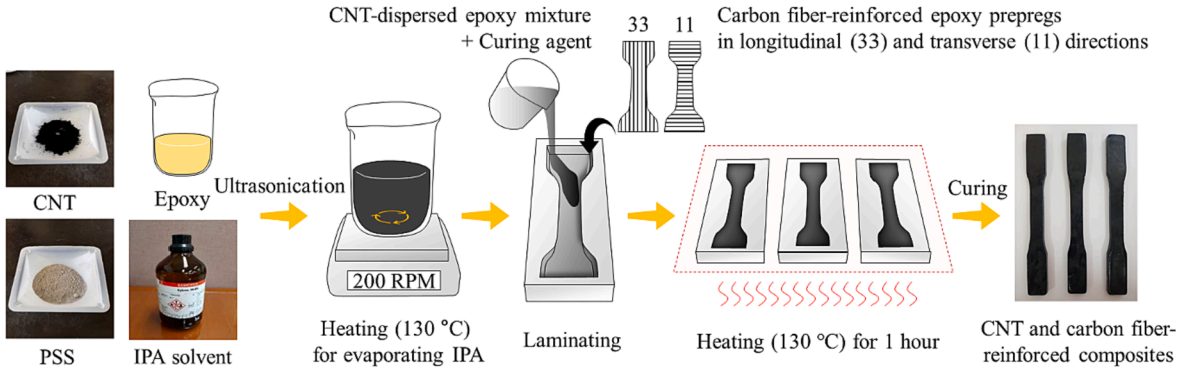

Fig. 6. Schematics of the fabrication procedure of the CNT and carbon fiber-reinforced composites.

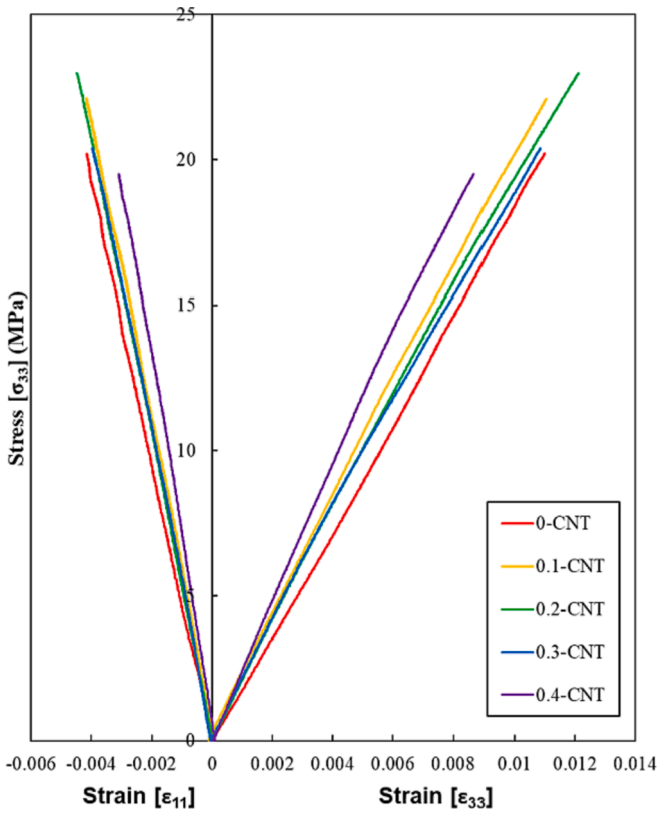

Fig. 7. Measured stress–strain behaviors of the CNT-reinforced composites.

composites. The predicted ν_{comp} value is increased slightly with an increase of the CNT content, while the ν_{comp} value from the experimental result varies in the range of 0.35 – 0.40. The standard deviations between the experimental and prediction values of E_{comp} and ν_{comp} are less than 5.0% for all composites. The assumption that CNTs are completely distributed in the polymer matrix is attributable to the discrepancy between the experimental results and the present predictions [33].

The predicted stress–strain behaviors of the CNT and carbon fiber-reinforced composites are compared with the experimental results. Fig. 9 shows the stress–strain behaviors in the longitudinal and transverse directions of the 0-CNT/CF composites, which are simulated with the fitted parameters through curve-fit to the present experimental results. The Weibull parameters ($S_{CF} = 1200$ and $M_{CF} = 1.0$) are fitted at the present experimental results of the 0-CNT/CF composites, and then the same values of the parameters are applied to the predictions of damage behavior of the 0.2-CNT/CF composites. The predicted values of E_{comp} and ν_{comp} in Fig. 8 are used for the CNT-reinforced composites, and the other parameters are identical to those used in Section 3.2. The comparisons of the stress–strain behaviors in the longitudinal and transverse directions of the 0.2-CNT/CF composites between the present experimental results and predictions with the fitted parameters obtained from Fig. 9 are shown in Fig. 10. Although the simulations for the composites under uniaxial tension are slightly lower than the corresponding experimental results, the present simulations are in good agreement with the experimentally measured stress–strain behaviors. These comparisons indicate that the proposed multi-level micromechanics-based homogenization could closely predict the stress–strain behaviors of CNT and carbon fiber-reinforced composites.

5. Concluding remarks

A multi-level micromechanics-based homogenization is proposed to predict the damage behavior of multiscale fiber-reinforced composites. A three-level homogenization process is suggested to estimate the effect of the effective molecular ellipsoidal inclusion orientation and geometry, carbon fiber orientation and volume fraction, and damage model parameters. The comparisons of the stress–strain behaviors of the

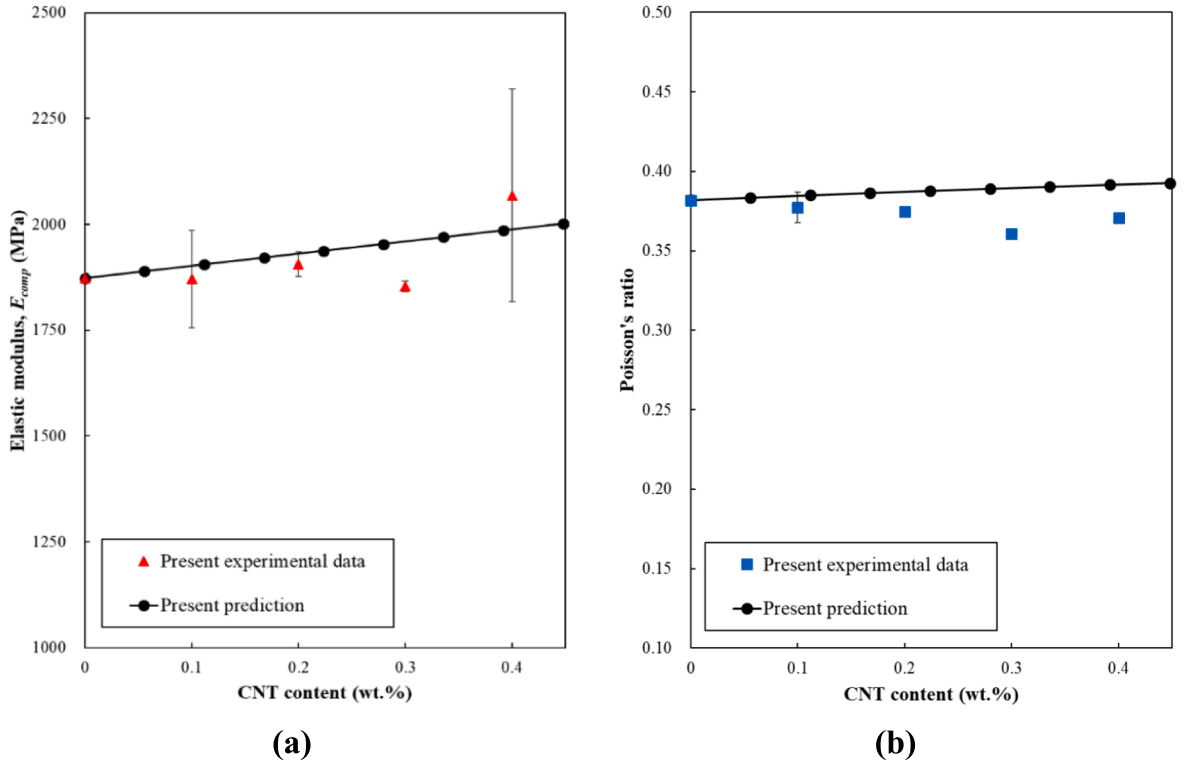

Fig. 8. Comparisons of (a) the elastic moduli and (b) Poisson's ratios of the CNT-reinforced composites between the experimental results and the present predictions.

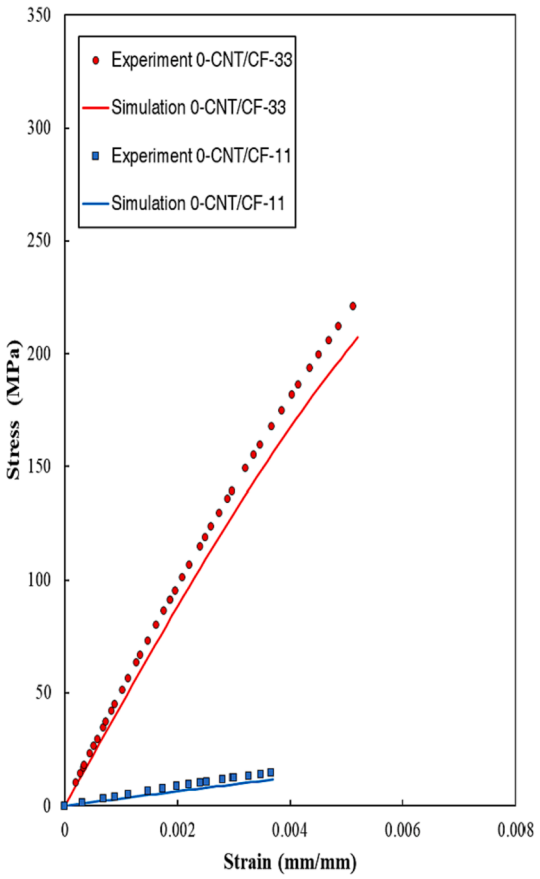

Fig. 9. The stress–strain behaviors of the 0-CNT/CF composites, which are simulated with the fitted parameters through curve-fit to the present experimental results.

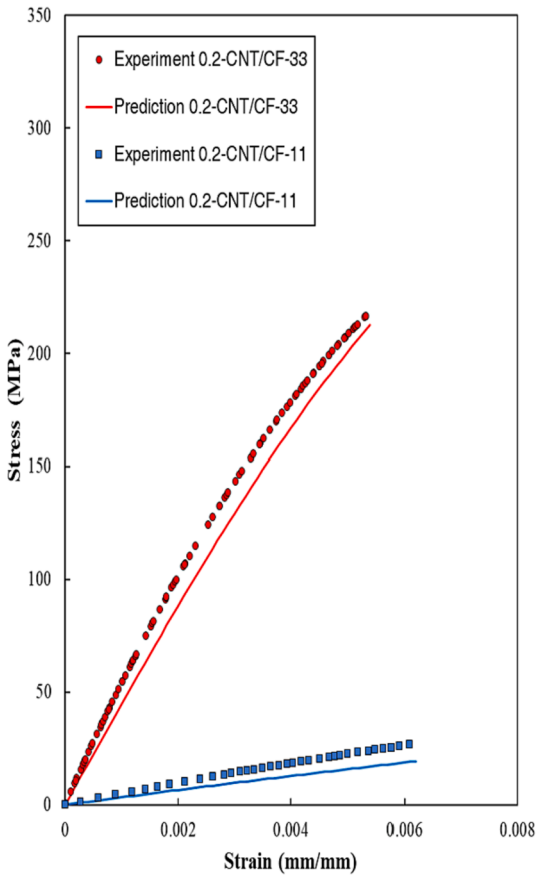

Fig. 10. Comparisons of the stress–strain behaviors in the longitudinal and transverse directions of 0.2-CNT/CF composites between the present experimental results and predictions with the fitted parameters obtained from Fig. 9.

composites between the experimental results and the present predictions are made to assess the predictive capability of the proposed framework. The findings from the present study can be summarized as follows.

(1) The assumption of the effective molecular ellipsoidal inclusion as the molecular unit cell is made in the present multi-level micromechanics-based homogenization. The predicted stress–strain behaviors of the CNT and carbon fiber-reinforced composites provide a close match to the experimental results.
(2) The orientation and aspect ratio of the effective molecular ellipsoidal inclusion affect the elastic modulus of the CNT-reinforced composites crucially. It is found that a higher aspect ratio of the inclusion which is aligned in the longitudinal direction results in a much higher stiffness of the composites.
(3) Higher values of the Weibull parameter S_{CF} lead to slower damage evolution of an imperfect interface in the longitudinal direction. On the other hand, the effects of the compliance parameters with the severely imperfect interfaces α_2 and β_2 on the damage behavior of the composites are notable in the transverse direction.

In order to evaluate the application of the present modeling scheme in a more accurate manner, additional experimental verifications on the composites with various nanoscale fiber materials (i.e., graphene, graphite, and carbon black) should be carried out. In addition, upscaling the present scheme for the implementation into a finite element program is needed to simulate various boundary value problems of multiscale fiber-reinforced composites on the macroscale.

CRediT authorship contribution statement

Taegeon Kil: Conceptualization, Methodology, Investigation, Resources, Writing – original draft. **Jin-Ho Bae:** Data curation, Visualization, Formal analysis. **Beomjoo Yang:** Software, Validation. **H.K. Lee:** Supervision, Project administration, Funding acquisition, Writing – review & editing.

Declaration of Competing Interest

The authors declare that they have no known competing financial interests or personal relationships that could have appeared to influence the work reported in this paper.

Data availability

No data was used for the research described in the article.

Acknowledgments

This research was supported by a grant from the National Research Foundation of Korea (NRF) funded by the Korean government (Ministry of Science, ICT & Future Planning) (NRF- 2021R1A2C3006382) and by a grant from Ministry of Land, Infrastructure and Transport (MOLIT) of Korea government and Korea Agency for Infrastructure Technology Advancement (KAIA) (21CTAP-C163988-01).

References

[1] Yao X, Falzon BG, Hawkins SC, Tsantzalis S. Aligned carbon nanotube webs embedded in a composite laminate: A route towards a highly tunable electro-thermal system. Carbon N Y 2018;129:486–94. https://doi.org/10.1016/j.carbon.2017.12.045.

[2] Lee HK, Simunovic S. A damage mechanics model of crack-weakened, chopped fiber composites under impact loading. Compos Part B Eng 2002;33(1):25–34.

[3] Nam IW, Park SM, Lee H-K, Zheng L. Mechanical properties and piezoresistive sensing capabilities of FRP composites incorporating CNT fibers. Compos Struct 2017;178:1–8.

[4] Joo S-J, Yu M-H, Kim WS, Kim H-S. Damage detection and self-healing of carbon fiber polypropylene (CFPP)/carbon nanotube (CNT) nano-composite via addressable conducting network. Compos Sci Technol 2018;167:62–70.

[5] Kil T, Jang DI, Yoon HN, Yang B. Machine learning-based predictions on the self-heating characteristics of nanocomposites with hybrid fillers. Comput Mater Contin 2022:71.

[6] Tafesse M, Alemu AS, Lee HK, Cho C-G, Kim H-K. Effect of chloride penetration on electrical resistivity of CNT–CF/cement composites and its application as chloride sensor for reinforced mortar. Cem Concr Compos 2022;133:104662.

[7] Kil T, Jin DW, Yang B, Lee HK. A comprehensive micromechanical and experimental study of the electrical conductivity of polymeric composites incorporating carbon nanotube and carbon fiber. Compos Struct 2021;268:114002.

[8] Cha J, Jun GH, Park JK, Kim JC, Ryu HJ, Hong SH. Improvement of modulus, strength and fracture toughness of CNT/Epoxy nanocomposites through the functionalization of carbon nanotubes. Compos Part B Eng 2017;129:169–79.

[9] Liu T, Phang IY, Shen L, Chow SY, De ZW. Morphology and mechanical properties of multiwalled carbon nanotubes reinforced nylon-6 composites. Macromolecules 2004;37:7214–22. https://doi.org/10.1021/ma049132t.

[10] Kil T, Jin DW, Yang B, Lee HK. A combined experimental and micromechanical approach to investigating PTC and NTC effects in CNT-polypropylene composites under a self-heating condition. Compos Struct 2022;289:115440.

[11] Jang D, Kil T, Yoon HN, Seo J, Khalid HR. Artificial neural network approach for predicting tunneling-induced and frequency-dependent electrical impedances of conductive polymeric composites. Mater Lett 2021;302:130420.

[12] Jia Y, Chen Z, Yan W. A numerical study on carbon nanotube pullout to understand its bridging effect in carbon nanotube reinforced composites. Compos Part B Eng 2015;81:64–71.

[13] Demczyk BG, Wang YM, Cumings J, Hetman M, Han W, Zettl A, et al. Direct mechanical measurement of the tensile strength and elastic modulus of multiwalled carbon nanotubes. Mater Sci Eng A 2002;334(1-2):173–8.

[14] Treacy MMJ, Ebbesen TW, Gibson JM. Exceptionally high Young's modulus observed for individual carbon nanotubes. Nature 1996;381(6584):678–80.

[15] Lee YM, You J, Kim M, Kim TA, Lee S-S, Bang J, et al. Highly improved interfacial affinity in carbon fiber-reinforced polymer composites via oxygen and nitrogen plasma-assisted mechanochemistry. Compos Part B Eng 2019;165:725–32.

[16] Abidin MSZ, Herceg T, Greenhalgh ES, Shaffer M, Bismarck A. Enhanced fracture toughness of hierarchical carbon nanotube reinforced carbon fibre epoxy composites with engineered matrix microstructure. Compos Sci Technol 2019;170:85–92.

[17] Kim GM, Yang BJ, Yoon HN, Lee HK. Synergistic effects of carbon nanotube and carbon fiber on heat generation and electrical characteristics of cementitious composites. Carbon N Y 2018;134:283–92. https://doi.org/10.1016/j.carbon.2018.03.070.

[18] Yang S, Yu S, Ryu J, Cho J-M, Kyoung W, Han D-S, et al. Nonlinear multiscale modeling approach to characterize elastoplastic behavior of CNT/polymer nanocomposites considering the interphase and interfacial imperfection. Int J Plast 2013;41:124–46.

[19] Alian AR, Kundalwal SI, Meguid SA. Multiscale modeling of carbon nanotube epoxy composites. Polymer (Guildf) 2015;70:149–60.

[20] Radue MS, Odegard GM. Multiscale modeling of carbon fiber/carbon nanotube/epoxy hybrid composites: comparison of epoxy matrices. Compos Sci Technol 2018;166:20–6.

[21] Kundalwal SI. Review on micromechanics of nano-and micro-fiber reinforced composites. Polym Compos 2018;39(12):4243–74.

[22] Rathi A, Kundalwal SI. Mechanical and fracture behavior of MWCNT/ZrO2/epoxy nanocomposite systems: experimental and numerical study. Polym Compos 2020;41(6):2491–507.

[23] Alian AR, Kundalwal SI, Meguid SA. Interfacial and mechanical properties of epoxy nanocomposites using different multiscale modeling schemes. Compos Struct 2015;131:545–55.

[24] Lee HK, Pyo SH. 3D-damage model for fiber-reinforced brittle composites with microcracks and imperfect interfaces. J Eng Mech 2009;135:1108–18. https://doi.org/10.1061/(asce)em.1943-7889.0000039.

[25] Jeon H, Yu J, Lee H, Kim GM, Kim JW, Jung YC, et al. A combined analytical formulation and genetic algorithm to analyze the nonlinear damage responses of continuous fiber toughened composites. Comput Mech 2017;60(3):393–408.

[26] Ju JW, Chen TM. Micromechanics and effective moduli of elastic composites containing randomly dispersed ellipsoidal inhomogeneities. Acta Mech 1994;103(1-4):103–21.

[27] Qu J, Cherkaoui M. Fundamentals of micromechanics of solids, vol. 92. Wiley Hoboken; 2006.

[28] Ju JW, Sun LZ. Effective elastoplastic behavior of metal matrix composites containing randomly located aligned spheroidal inhomogeneities. Part I: micromechanics-based formulation. Int J Solids Struct 2001;38:183–201.

[29] Pyo SH, Lee H-K. Micromechanical analysis of aligned and randomly oriented whisker-/short fiber-reinforced composites. Comput Model Eng Sci 2009;40:271.

[30] Pyo SH, Lee HK. Micromechanics-based elastic-damage analysis of laminated composite structures. Int J Solids Struct 2009;46(17):3138–49.

[31] Yang BJ, Ha SK, Pyo SH, Lee HK. Mechanical characteristics and strengthening effectiveness of random-chopped FRP composites containing air voids. Compos Part B Eng 2014;62:159–66.

[32] Qu J. Eshelby tensor for an elastic inclusion with slightly weakened interface 1993.

[33] Haile BF, Jin DW, Yang B, Park S, Lee HK. Multi-level homogenization for the prediction of the mechanical properties of ultra-high-performance concrete. Constr Build Mater 2019;229:116797.

[34] Lee HK, Pyo SH. Multi-level modeling of effective elastic behavior and progressive weakened interface in particulate composites. Compos Sci Technol 2008;68(2):387–97.

[35] Weibull W. A statistical distribution function of wide applicability. J Appl Mech 1951;18:293–7.

[36] Ju JW, Lee HK. A micromechanical damage model for effective elastoplastic behavior of partially debonded ductile matrix composites. Int J Solids Struct 2001;38(36-37):6307–32.

[37] Karihaloo BL, Fu D. A damage-based constitutive law for plain concrete in tension. Eur J Mech A Solids 1989;8:373–84.

[38] Liang Z, Lee HK, Suaris W. Micromechanics-based constitutive modeling for unidirectional laminated composites. Int J Solids Struct 2006;43(18-19):5674–89.

[39] Han Y, Elliott J. Molecular dynamics simulations of the elastic properties of polymer/carbon nanotube composites. Comput Mater Sci 2007;39(2):315–23.

[40] Jang D, Yoon HN, Nam IW, Lee HK. Effect of carbonyl iron powder incorporation on the piezoresistive sensing characteristics of CNT-based polymeric sensor. Compos Struct 2020;244:112260.

[41] International A. ASTM D638-14, Standard Test Method for Tensile Properties of Plastics. ASTM International; 2015.

[42] Panchagnula KK, Kuppan P. Improvement in the mechanical properties of neat GFRPs with multi-walled CNTs. J Mater Res Technol 2019;8(1):366–76.

[43] Kim GM, Kil T, Lee HK. A novel physicomechanical approach to dispersion of carbon nanotubes in polypropylene composites. Compos Struct 2021;258:113377.

[44] Hu N, Li Y, Nakamura T, Katsumata T, Koshikawa T, Arai M. Reinforcement effects of MWCNT and VGCF in bulk composites and interlayer of CFRP laminates. Compos Part B Eng 2012;43(1):3–9.

[45] Materials ACD-30 on C. Standard test method for tensile properties of polymer matrix composite materials. ASTM international; 2008.

[46] Gojny FH, Wichmann MHG, Köpke U, Fiedler B, Schulte K. Carbon nanotube-reinforced epoxy-composites: enhanced stiffness and fracture toughness at low nanotube content. Compos Sci Technol 2004;64(15):2363–71.